MDH2 is a metabolic switch rewiring the fuelling of respiratory chain and TCA cycle

Thibaut Molinié[1], Elodie Cougouilles[1], Claudine David[1], Edern Cahoreau[2,3], Jean-Charles Portais[2,3,4], Arnaud Mourier[1*].

[1] Univ. Bordeaux, CNRS, IBGC, UMR 5095, F-33000 Bordeaux, France
[2] TBI, Université de Toulouse, CNRS, INRA, INSA, Toulouse, France
[3] MetaToul-MetaboHUB, National infrastructure of metabolomics and fluxomics, Toulouse, France
[4] RESTORE, INSERM U1031, CNRS 5070, UPS, EFS, Toulouse, France

*Correspondence:
Arnaud Mourier
Institut de Biochimie et de Génétique Cellulaires
CNRS-UMR5095
1, rue Camille Saint-Saëns
CS 61390
33077 Bordeaux cedex
France
arnaud.mourier@ibgc.cnrs.fr

RUNNING TITLE
Malate-aspartate shuttle orchestrates respiratory chain electron flow

SUMMARY

The mitochondrial respiratory chain (RC) enables many metabolic processes by regenerating both mitochondrial and cytosolic NAD^+ and ATP. In contrast to ADP, NADH metabolically produced in the cytosol is not transported across the inner mitochondrial membrane and must be indirectly transferred inside mitochondria through the malate-aspartate shuttle (MAS) to fuel RC with electrons. MAS is the major pathway maintaining cytosolic NADH/NAD^+ redox balance in mammalian tissues such as liver and heart and its activity is crucial for cell metabolism, division and survival. However, the specific metabolic regulations allowing mitochondrial respiration to prioritize NADH oxidation in response to high NADH/NAD^+ redox stress have not been elucidated. The recent discovery that complex I (NADH dehydrogenase), and not complex II (Succinate dehydrogenase), can assemble with other RC complexes to form functional entities called respirasomes, led to the assumption that this supramolecular organisation would favour NADH oxidation. Surprisingly, our bioenergetic characterization of liver and heart mitochondria demonstrates that the RC systematically favours electrons provided by complex II. However, mitochondrial malate dehydrogenase (MDH2) mediated metabolic regulation can rewire respiratory chain electrons flow from succinate toward NADH oxidation in response to increase MAS activity. Interestingly, this new regulatory mechanism synergistically increases RC's NADH oxidative capacity and rewires MDH2 driven anaplerosis of the TCA, preventing malate production from succinate to favor oxidation of cytosolic malate. This discovery demonstrates that MAS does not only passively balance cytosolic and mitochondrial NADH but instead, in response to cytosolic redox stress, MAS actively rewires RC's fuelling, inhibiting complex II to prioritize cytosolic NADH oxidation and increase complex I oxidative capacity.

HIGHLIGHTS

- Heart and liver respiratory chains preferentially oxidize succinate.
- The preferential succinate oxidation is independent of the relative abundance of complex I and II.
- MDH2 mediated feedback inhibition of complex II can counteract the preferential succinate oxidation to increase NADH oxidative capacity.
- The malate-aspartate shuttle inhibits mitochondrial conversion of succinate into malate to prioritize the mitochondrial oxidation of cytosolic malate.

KEYWORDS

Mitochondria, bioenergetics, MDH2, oxaloacetate, malate aspartate shuttle, NADH redox homeostasis, respiratory chain supercomplexes, respirasomes

INTRODUCTION

Mitochondria are organelles present in almost all eukaryotic cells and are essential for the maintenance of cellular metabolism. The OXPHOS system, which is located in the inner mitochondrial membrane (IMM), is composed of two functional entities: the respiratory chain (RC) and the phosphorylation system, which includes the ATP synthase and carriers, such as the ATP/ADP carrier and the phosphate carrier (Chance and Williams, 1956). Historically, the mitochondrial respiratory chain has been defined as an ensemble of four protein complexes (I, II, III, and IV) and of mobile electrons carriers as coenzyme Q (CoQ) and cytochrome-*c* (Cyt *c*). In contrast to complex II, complexes I, III, and IV are defined as coupling sites as they couple redox reactions to proton translocation outside the matrix space. The protons electrochemical potential generated across the IMM by the RC, allows the ATP synthase (complex V) to generate ATP (Mitchell, 1961). Beyond ATP synthesis, mitochondrial maintenance of NADH/NAD^+ redox cofactor balance is of paramount importance for numerous mitochondrial and cytosolic metabolic pathways (Alkan et al., 2020; Borst, 2020; Lee et al., 2020). As direct import of reduced coenzyme NADH is prevented by the selective permeability of IMM (Purvis and Lowenstein, 1961), redox shuttles as the Malate Aspartate Shuttle (MAS), or the α-glycerophosphate shuttle are required to allow mitochondrial RC to indirectly oxidize the cytosolic NADH produced by glycolysis and other metabolic pathways (Cederbaum et al., 1973; Dawson, 1979; Safer et al., 1971). The MAS has been demonstrated to be the predominant NADH redox shuttle in highly oxidative tissues as brain, heart and liver (LaNoue et al., 1973, 1974). This key redox shuttle involves mitochondrial carriers as well as cytosolic and mitochondrial malate dehydrogenases (MDH1, MDH2) and glutamate aspartate transaminases (GOT1, GOT2) (Borst, 2020). Intercompartment metabolite cycling through the MAS allows MDH1 and MDH2 to work in opposite directions (oxidizing cytosolic NADH and

reducing mitochondrial NAD^+) enabling complex I to indirectly oxidize cytosolic NADH (Figure 4A).

Beyond NADH redox shuttles (Complex I and mG3PDH), several other oxidoreductases feed the RC at the level of coenzyme Q, complex II (TCA cycle), ETF (β-oxidation), SQOR (sulfide metabolism) and DHODH (pyrimidine synthesis) subjugating *de facto* these key metabolic pathways to RC activity (Devin et al., 2019; Kohl et al., 2019). The fact that all these dehydrogenases rely on CoQ as common substrate, prompted scientists to investigate molecular processes orchestrating this CoQ contest in different model organisms (Bunoust et al., 2005; Lapuente-Brun et al., 2013; Mourier et al., 2010; Påhlman et al., 2001). A recent burst of interest in understanding regulation and activity of CoQ oxidoreductases was triggered by recent evidence that in contrast to Complex II, the vast majority of Complex I physically interact with other RC complexes III and IV (Schägger and Pfeiffer, 2000). One of the most important arguments for a higher order organization of the respiratory chain was provided by the use of blue native polyacrylamide gel electrophoresis (BN-PAGE), which showed that respiratory chain complexes from a wide range of organisms can be extracted in supramolecular assemblies when mitochondria are solubilized using mild detergents (Schägger and Pfeiffer, 2000). In mammalian mitochondria, supercomplexes (SCs) consisting of complexes I, III, and IV are functional entities consuming oxygen in presence of NADH and are therefore named respirasome (Acín-Pérez et al., 2008; Dudkina et al., 2010; Schägger and Pfeiffer, 2000). Recent studies using a multitude of independent approaches, such as electron cryo-microscopy (cryo-EM) (Gu et al., 2016; Letts et al., 2016), electron cryo-tomography (cryo-ET) (Davies et al., 2018), cross-linking mass spectrometry (Chavez et al., 2018), and Förster resonance energy transfer (FRET) analyses (Rieger et al., 2017), have convincingly proven existence of respirasomes in various organisms. Respirasomes have been reported to play a critical role in bioenergetics and proposed to sequester dedicated pools of CoQ and Cyt

c in order to function as independent bioenergetic units. It has also been proposed that respirasome could reduce the diffusion distance of CoQ and Cyt *c*, thereby increasing the electron transfer efficiency between complexes organized in respirasomes (Balsa et al., 2019; Bianchi et al., 2004; Lapuente-Brun et al., 2013). However, analyses of supercomplex structures, as well as of kinetic and spectroscopic data, do not support substrate channelling by sequestration of CoQ and Cyt *c* (Blaza et al., 2014; Fedor and Hirst, 2018; Trouillard et al., 2011). Therefore, the bioenergetic roles of respirasomes on mitochondrial NADH oxidation efficiency and on prioritizing electron delivered by complex I against other respirasome-free CoQ-oxidoreductases remain in question.

In this study, we carefully characterize the bioenergetic properties of heart and liver murine mitochondria, as their metabolism strongly depend on MAS (LaNoue et al., 1973; Safer B, 1975), but also differ in their respective capacity to oxidize NADH versus succinate (Brandt et al., 2017). We developed independent cell-free biochemical approaches to decipher molecular mechanisms orchestrating complex I and II activities when the demand in oxidizing both NADH and succinate is high. In contrast with the kinetic advantage allegedly conferred to NADH oxidation by the assembly of complex I into respirasomes, our results show that succinate oxidation is prioritized over NADH oxidation, in both liver and heart mitochondria. However, we demonstrated that MDH2 mediated metabolic regulation rewires RC electrons flow priority from succinate toward NADH oxidation. This MDH2 mediated metabolic regulation concomitantly rewire RC and anaplerosis of TCA cycle, downregulating malate production to favour oxidation of cytosolic malate. Consequently, MAS does not just passively balance NADH/NAD^+ redox between cytosol and mitochondria, but actively rewires RC electron flow and TCA cycle activity, increasing mitochondrial NADH oxidation capacity when cytosolic NADH oxidation demand is high.

RESULTS AND DISCUSSION

Heart and liver mitochondria strongly differ in their NADH and succinate oxidative capacities

To elucidate how mitochondrial RC orchestrates NADH and succinate oxidation we characterized heart and liver mitochondria presenting high TCA and MAS metabolic activities. Bioenergetic characterization of isolated heart and liver mitochondria was performed by measuring the oxygen consumption under phosphorylating, non-phosphorylating and uncoupled conditions using high-resolution O2K oxygraphs. To determine the capacity of heart and liver mitochondria to oxidize NADH or succinate, metabolically active mitochondria were incubated in the presence of various nutrient combinations whose metabolism results in delivery of electrons at the level of complex I or complex II. In both heart and liver, we found that simultaneous addition of pyruvate, glutamate and malate was the best combination of nutrient to feed complex I with electrons (Figure S1A-B). Then, we confirmed that adding complex I inhibitor (rotenone) in presence of succinate was essential to assess maximal complex II driven respiration (Figure S1C-D). In line with previous observations (Brandt et al., 2017), respirations assessed under phosphorylating or uncoupled conditions were 5 to 3 times higher in heart than in liver mitochondria (Figure 1A-B). Furthermore, our analyses showed that, compared to the succinate driven respiration, heart mitochondria present higher complex I driven respiration (Figure 1A) than liver mitochondria (Figure 1B). This observation prompted us to decipher if the observed difference in complex I and II driven respirations, was caused by mitochondrial metabolic constraint affecting NADH or succinate provisional of the RC or to intrinsic RC functional discrepancies. To this end, we permeabilized mitochondria to specifically measure RC activity fed directly with NADH or succinate. Interestingly, when RC is fuelled ad libitum with reduced substrates, heart RC can oxidize NADH two time faster than succinate (Figure 1C) whereas an opposite situation is observed in liver RC (Figure 1D). The high disparity in NADH and succinate oxidation rates observed between heart and liver RC

prompted us to further characterize tissue specific RC composition changes. To this end, we quantified RC complex levels assessing cytochromes (Figure 1E) and proteins contents (Figure 1F-H). These two independent approaches consistently showed that all cytochromes as well as RC complex subunits were two to four time more abundant in heart compared to liver mitochondria (Figure 1E-G). Moreover, the relative abundance of complex I normalized to complex II was almost tripled in heart compared to liver (Figure 1H). Altogether, the data presented in Figure 1 show that RC complexes content and stoichiometry strongly differ between heart and liver (Figure 1 E-H) and that these differences correlate with tissue specific functional differentiation (Figure 1 A-D). Interestingly, when both complex I and complex II substrates are added to mitochondria, the increase in RC activity is too low to sustain both NADH and succinate oxidation flow at maximal speed (Figure 1A-D). This observation prompted us to develop assays allowing to determine the respective contribution of complex I and complex II in feeding RC with electrons, when both NADH and succinate are present.

Heart and liver respiratory chain preferentially oxidize succinate over NADH

The respective contribution of NADH and succinate oxidation in fuelling RC with electrons when mitochondria are in presence of both substrates, was first evaluated using validated and highly specific complex I or II inhibitors *i.e.* rotenone (Rot) and Atpenin A5 (AtpnA5) (Figure S2A-D). Interestingly, this inhibitor driven approach consistently demonstrates that when permeabilized mitochondria are incubated with both NADH and succinate, complex II driven respiration was preserved whereas complex I driven respiration was strongly and significantly decreased in heart and liver mitochondria (Figure 2A-B). This significant downregulation of complex I activity in presence of succinate, was confirmed by enzymatic measurement of the NAD^+ production rate (Figure 2C-D). Interestingly, despite the great disparity in their respective complex I and II oxidative capacities (Figure 1C-D), the

priority given to complex II electrons, was consistently observed in both heart and liver mitochondria (Figure 2A-D).

The finding that liver and heart RC preferentially oxidize succinate over NADH was in stark contrast to recent hypothesis supporting the fact that the structural association of complex I with complex III and IV should confer kinetics advantage to NADH oxidation over electrons provided by the respirasome free complex II (Enríquez, 2016; Lapuente-Brun et al., 2013). This surprising result prompted us to investigate the supramolecular organization of heart and liver RC. To this end, mitochondria were solubilized using digitonin (at a ratio of 3 g digitonin per g protein) and the supramolecular organization of the RC was then resolved using standard BN-PAGE technique and analyzed by western blotting or in-gel activity assay (Figure 2E-F, Figure S2E-G). First, BN-PAGE profiles presented in the Figure 2E and 2F clearly confirmed the striking enrichment of heart RC in complex I and IV compared to liver RC, supporting our previous observations (Figure 1E-G). Interestingly, these changes in RC complexes stoichiometry between the two tissues, remarkably correlate the abundance and diversity of respirasomes (IxIIIyIVz) (Figure 2E-F). To determine the proportion of complex I and II assembled in supercomplexes, BN-PAGE first dimension were further resolved in a second denaturing dimension. 2D-BN-PAGE is commonly used to properly detect and quantify the presence of a protein as they prevent potential epitope accessibility issues often encountered when western blot is directly performed in conditions preserving proteins' tertiary and quaternary structures. Remarkably, 2D electrophoresis analyses were in agreement with previous studies (Greggio et al., 2017; Schägger and Pfeiffer, 2001) showing that more than 90% of heart and liver complex I are found associated in respirasomes whereas no detectable complex II could be found associated in supercomplexes (Figure 2E-I, Figure S2E-G). Furthermore, the supramolecular organization of complex I and II with other RC is not plastic as no respirasome reshuffling could be observed when BN-PAGE experiments were performed

solubilizing mitochondria actively metabolizing different respiratory substrates (Figure S2H-I). Altogether, our results indicate that despite the absence of physical interaction between complex II and other RC complexes, succinate oxidation is prioritized over electrons delivered by complex I.

Internal oxaloacetate level orchestrates the respective contribution of complex I and II to respiration

To evaluate potential metabolic outcomes of the preferential succinate oxidation on TCA and MAS cycle activities, we applied our new experimental strategy deciphering the origin of electrons fuelling the RC on intact and metabolically active mitochondria. In intact mitochondria, succinate is transported through dicarboxylate carrier before being directly oxidized by complex II. In contrast, NADH cannot be directly imported and will have to be metabolically generated from matrix dehydrogenases like malate, glutamate or pyruvate dehydrogenases. Use of specific inhibitor demonstrated that mitochondrial respiration assessed in presence of pyruvate, glutamate, and malate (PGM) totally rely on complex I activity as this respiration was abolished by rotenone (Figure S2A-C). Similarly, succinate driven respiration was inhibited in presence of AtpeninA5 (Figure S2B-D). Interestingly, uncoupled respiration assessed in presence of succinate and rotenone (Figure 3A-B) are almost identical to succinate driven respiration measured on permeabilized mitochondria (Figure 2A-B). However, when succinate driven uncoupled respiration is assessed in absence of rotenone, respiration values are decreased by 40% in heart and 30% in liver mitochondria (Figure 3A-B and Figure S1C-D). The necessity to add rotenone to assess maximal succinate driven respiration on metabolically active mitochondria has been explained as complex I inhibition could prevent accumulation of oxaloacetate (OAA) a potent competitive inhibitor of complex II (Fink et al., 2018; Gnaiger, 2009; Schollmeyer and Klingenberg, 1961). To characterize the specificity and the metabolic relevance of OAA inhibition, permeabilized mitochondria incubated with

succinate or NADH were recorded in presence of increasing concentration of OAA (Figure S3A). These analyses clearly demonstrated that OAA is a powerful and highly specific complex II inhibitor, as no inhibitory side effects could be observed on NADH driven respiration. To elucidate the potential regulatory function of OAA on succinate respiration in intact mitochondria, we developed an enzymatic assay to quantify OAA levels (Figure 3C-D). Our analyses performed on both heart and liver mitochondria confirmed that the stimulation of succinate respiration by rotenone (Figure 3A and B) was associated with a striking lowering of OAA level (Figure 3C-D). As expected, extemporaneous fluorometric measurement of mitochondrial internal NAD(P)H level demonstrated that inhibition of complex I by rotenone provoked a massive increased of mitochondrial redox (NAD(P)H) state (Figure 3E, Figure S3B). Interestingly, NMR spectroscopy analyses showed that treatment of succinate-metabolizing mitochondria with rotenone, provoked a massive excretion of malate and fumarate (Figure 3F). Altogether, our analyses support that the massive increase in $NADH/NAD^+$ ratio secondary to complex I inhibition by rotenone could prevent MDH2 driven OAA production (Figure 3C-D) which consequently increases succinate respiration (Figure 3A-B).

To determine the respective contribution of complex I and II in fuelling RC with electrons on intact mitochondria, we applied the inhibitor-driven approach. This approach was validated on intact mitochondria as rotenone and atpeninA5 sensitive respirations, assessed under uncoupled conditions, were additive and independent of the sequence of addition of inhibitors (figure S3C-D). Intriguingly, in contrast to the results obtained on permeabilized mitochondria (Figure 2A-B), complex I dependent respiration was preserved in presence of multiple substrates, whereas complex II respiration was similar or even lower than the 'OAA inhibited' succinate respiration measured in absence of rotenone (Figure 3A-B). Interestingly, the OAA levels perfectly matched the degree of inhibition of the succinate respiration when all

substrates were provided to heart (Figure 3C) and liver (Figure 3D) mitochondria. Altogether, our data identified OAA as a key metabolic regulator orchestrating the respective contribution of complex I and II to RC electron flow. The OAA regulation occurring in intact mitochondria could totally counteract the natural RC priority given to complex II, to favour NADH oxidation.

MDH2 is a metabolic switch rewiring respiratory chain and TCA fuelling

The importance of MDH2-generated OAA in orchestrating mitochondrial NADH or succinate oxidation, prompted us to investigate the metabolic relevance of this new regulatory mechanism. MDH2 is a mitochondrial metabolic checkpoint located at the crossroad of TCA cycle and MAS (Figure 4A). To decipher the functional interplay between MAS, RC and TCA cycle, we assessed complex II driven respiration mimicking increasing cytosolic NADH re-oxidation demand by increasing external malate concentration (Figure 4A) (Safer et al., 1971). This experiment demonstrated that complex II driven respiration decreased proportionally in response to increased malate concentration (Figure 4B-D, S4A-C). As control, we showed that malate *per se* did not impact succinate respiration in permeabilized mitochondria (Figure S4D). This observation further explained why malate inhibition only occurred in metabolically active mitochondria where OAA can be generated and accumulated. In line with this observation, the decrease in complex II driven respiration associated with increase malate concentration was perfectly correlated with an increase in mitochondrial OAA level (Figure 4D and S4C). Altogether, our data show that more than 60% of complex II driven respiration can be downregulated in response to cytosolic redox stress through a MDH2-mediated metabolic regulation in both heart and liver.

To confirm that OAA could act as mitochondrial metabolic sensor adjusting RC fuelling to mitochondrial metabolic activity, we investigated how OAA consuming pathways impact succinate and NADH dependent respirations. To this end, mitochondrial RC activity was assessed in presence of succinate (Succ) and glutamate (Glu) or/and pyruvate (Pyr) to

metabolically flush OAA through MAS (GOT2 dependent pathway) or through the TCA cycle (pyruvate dehydrogenase and citrate synthase dependent pathway) (Figure 4A). Our analyses demonstrated that both pyruvate and glutamate are efficient in consuming internal OAA as both substrates added alone or in combination can lower OAA to similar residual level as the one measured in succinate and rotenone condition (Figure 4E and S4E). The metabolic flush of OAA was not only increasing succinate driven respiration by releasing complex II inhibition, but it also fuelled complex I with NADH (Figure 4F and S4F). Eventually, we decided to determine if MDH2 could metabolically rewire RC electrons entry from succinate toward NADH, when MAS driven external NADH oxidation demand is increased (increasing malate concentration within physiological range). Our results clearly showed that Malate-OAA dependent respiration rewiring from complex II to complex I occurs, even when OAA produced by the MDH2 can be metabolically flushed through MAS and TCA cycle (Figure 4G). Remarkably, imported malate oxidized through MDH2 not only downregulates succinate driven respiration, but it also increases MDH2 NADH production and complex I driven NADH oxidation capacity.

CONCLUSION

The recent discovery that complex I, and not complex II, assemble with other RC complexes to form respirasomes, led to the assumption that this supramolecular organisation would favour NADH oxidation. Surprisingly, our bioenergetic characterization of liver and heart mitochondria demonstrates that the RC systematically favours electrons provided by complex II. This key observation underscored the importance of OAA, acting as a specific and reversible inhibitor of complex II in intact mitochondria. Remarkably, our results demonstrate that succinate driven respiration is tightly controlled by OAA levels, rewiring RC fuelling from succinate toward NADH. This new regulatory mechanism synergistically increases RC's

NADH oxidative capacity and rewires MDH2 driven TCA anaplerosis, preventing malate production from succinate to favour oxidation of cytosolic malate to increase MAS activity. This discovery demonstrates that MAS does not only passively balance cytosolic and mitochondrial NADH but instead, in response to cytosolic redox stress, MAS actively rewires RC's fuelling, inhibiting complex II to prioritize cytosolic NADH oxidation and increase complex I oxidative capacity.

EXPERIMENTAL PROCEDURES

Biological materials

All mice used in this study were on an inbred C57Bl/6N background. Mice were maintained on a standard mouse chow diet and sacrificed, between 20 and 40 weeks of age, by cervical dislocation in strict accordance with the recommendations and guidelines of the Federation of the European Laboratory Animal Science Association, and obtain with an authorization from the French ministry of Agriculture (APAFIS#12648-2017112083056692v7).

Heart and liver mitochondria Isolation

Isolation of heart and liver mitochondria was performed by differential centrifugation as previously described (Brandt et al., 2017; Mourier et al., 2015). Briefly, right after the sacrifice, tissues were collected, minced and cleaned with mitochondria isolation buffer (MIB; 310 mM sucrose, 20 mM Tris-Base, 1 mM EGTA, pH 7.2) for the heart and MIB+BSA (MIB and 0.25mg/ml of delipidated Bovine serum albumin (BSA)) for the liver. The pieces of heart were collected and homogenized with few strokes of a Potter S homogenizer (Sartorius) using a loose Teflon pestle, in an ice cold MIB supplemented with trypsine (0.5 g/l). Liver tissues homogenisation was performed in a Potter S homogenizer (Sartorius) using a Teflon pestle, and in ice cold MIB+BSA. Mitochondria were isolated by differential centrifugation, a low speed one (1,000g, 10 min, 4C) in a swing out rotor and another one at high speed (3,500g, 10 min, 4°C for heart mitochondria and 10,000g, 10 min, 4C for liver mitochondria) using a fixed angle rotor. The pellet of crude mitochondria obtained is suspended in MIB+BSA. Protein concentration was measured using Bio-Rad DC Protein Assay kit according to provider's instructions.

High-resolution oxygen consumption measurement

Oxygen consumption of intact crude mitochondria was measured at 37°C, using respectively 50µg and 100µg of heart and liver mitochondria diluted in 2.1ml of respiratory

buffer (RB : 120 mM sucrose, 50 mM KCl, 20 mM Tris-HCl, 4 mM KH_2PO_4, 2 mM $MgCl_2$, 1 mM EGTA, 0.25 mg/ml delipidated BSA; pH 7.2) in an Oxygraph-2k (OROBOROS INSTRUMENTS, Innsbruck, Austria) (Mourier et al., 2014). Oxygen consumption was measured by using different association of substrates: succinic acid (5 mM; pH7.2), sodium pyruvate (10 mM; pH7.2), L-Glutamate acid (10 mM; pH7.2), L-Malic acid (concentrations are indicated in the figure legends; pH7.2). Oxygen consumption rate was measured under 3 different conditions: in the phosphorylating state with addition of ADP (5 mM; pH7.2), in the non-phosphorylating state with addition of oligomycin (50 ng/ml), and in the uncoupled state by successive addition of carbonyl cyanide m-chlorophenyl hydrazone (CCCP) up to 0.5 µM to reach the maximal respiration of the RC.

Activity of the RC was also recorded using permeabilized crude mitochondria obtain after freeze and thaw cycle. Oxygen consumption by the RC was measured as previously described (Mourier et al., 2014), using respectively 50 and 100µg of heart and liver mitochondria diluted in 2.1ml of potassium phosphate buffer (50 mM, pH 7.2) and incubated with saturating concentrations of cytochrome *c* (62.5 µg/ml), NADH (0.625 mM) and succinate (10 mM) . No oxygen consumption could be detected in absence of cytochrome *c*, and no oxygen consumption link to complex I activity was recorded when permeabilized mitochondria are incubated with pyruvate, glutamate and malate, confirming the loss of integrity of mitochondrial internal compartment.

The determination of oxygen consumption link to electron coming from complex I and complex II was determined after addition of rotenone (Rot, 30 nM) for complex I and/or atpenin A5 (AtpnA5, 20nM) for complex II. As a control, Antimycin A (100 nM) was added at the end of each experiment to control the proportion of oxygen consumption which is not linked to RC.

Mitochondrial cytochromes quantification

The different cytochromes of the mitochondrial respiratory chain were measured by dual-wavelength spectrophotometry by comparing the spectra of fully oxidized *vs*. fully reduced cytochromes. In each of the two cuvettes, 2 mg of heart or 16 mg of liver mitochondrial protein were suspended in 1 ml of phosphate buffer (50 mM, pH 7.2), and 0.05% (vol/vol) Triton X-100 were added. In the "oxidized" cuvette, 10 µl of ferricyanide (0.5 M) were added while a few grains of sodium hydrosulfite were added in the "reduced" cuvette. The components were mixed, and the absorbance spectrums of both cuvettes were recorded. A typical difference between reduced minus oxidized spectra was obtained. Wavelength pairs and absorption coefficient used were: cytochrome *c* + *c1* (550–540 nm) ε = 18 mM^{-1}/cm, cytochrome *b* (563–575 nm) ε = 18 mM^{-1}/cm and cytochrome *a* + *a3* (605–630 nm) ε = 24 mM^{-1}/cm.

Western-blot analyses

Proteins from crude heart and liver mitochondria were resolved using denaturing (SDS PAGE or native electrophoreses (BN-PAGE and Second dimensional SDS PAGE)).

For SDS PAGE, 50 µg of heart and liver crude mitochondria proteins were solubilised with RIPA buffer (NaCl (150 mM), tris-base (25 mM), NP40 (1% w/v), SDS (1% w/v), deoxycholate (0.25% w/v) et d'EGTA (1 mM), pH 8). Solubilised mitochondria were mixed with Laemmli buffer (Laemmli, 1970), separated by Bis-Tris 15% acrylamide gel, and then transferred on nitrocellulose Amersham Protran Premium membrane (Amersham). Immunodetection was performed by fluorescence using a Typhoon FLA 9500 (GE Healthcare Life Sciences). To perform immunodetection, membranes were blocked with 3% (w/v) milk diluted in Tris Buffer Saline (TBS; pH 8), then primary antibody (Total OXPHOS Rodent WB Antibody Cocktail; Abcam) was added for incubation, and finally an ECL Plex™ G-A-R IgG, Cy®5 (GE Healthcare) anti-mouse secondary antibody was used. The FIJI software was used to determine and analyse densitometric profiles.

BN-PAGE analyses

For BN-PAGE, 50 µg of crude heart mitochondria and 150 µg of crude liver mitochondria proteins were incubated with digitonin extraction buffer (HEPES (30 mM), potassium Acetate (150 mM), Glycerol (12%), 6-Aminocaproic acid (2 mM), EDTA (2 mM), high-purity digitonin (3 g/g), pH 7.2), and vortexed 1h at 4°C to solubilize membranes. After incubation, mitochondria were centrifugated at 30,000 g for 20 minutes, supernatants were collected and mixed with loading dye (0.0125% (w/v), Coomassie brilliant blue G-250). Native complexes were resolved using Bis-Tris Invitrogen™ Novex™ NativePAGE™ 3-12% or 4-16% acrylamide gradient. To reach the optimal separation and resolution of OXPHOS supramolecular organisations, digitonine solubilised proteins were loaded on 3-12% gradient gel and were migrated at 10 mA for 12 h at 4°C (complex II are not retained in the gel after overnight run). To analyse the complex II assembly, 4-16% gradient gels were migrated 6 h in order to keep the complex II in gel and for optimal separation of OXPHOS SC. OXPHOS complexes were detected using in-gel activity (IGA) assays as described previously (Wittig et al.). Briefly, native gels were washed and incubated in a potassium phosphate buffer (50 mM, pH 7.2) containing iodonitrotetrazolium (1 mg/ml) supplemented with NADH (400 µM, pH7.2) for complex I or Succinate (50 mM, pH7.2) and Phenazine Methosulfate (20mM) for complex II. For complex IV in-gel activity assays, native gels were incubated in RB containing Diaminobenzidine (1 mg/ml) and cytochrome *c* (0.5 mg/ml). Coomassie staining was performed with PageBlue protein staining solution. Colorimetric bands were recorded with Optical Densitometry of an Amersham ImageQuant 800.

Proteins were also immunodetected, gels were incubated in Towbin buffer (Tris (0.3% p/v), Glycine (0.44% p/v), Ethanol (10% v/v)) supplemented with SDS (0.2% v/v) and β-mercaptoethanol (0.2% v/v) for 30 minutes at RT, to denature proteins. Then gels were transferred on polyvinylidene difluoride (PVDF) in Towbin transfer buffer for 2h at 0.2 A.

Immunodetection was performed as described previously, peroxidase-conjugated anti-mouse and anti-rabbit IgGs and Amersham CyDye 800 goat anti-rabbit and anti-mouse were used for immunodetection by chemiluminescence and fluorescence. Immunoreactive bands were recorded with an Amersham ImageQuant 800.

BN-PAGE gels after first dimension electrophoresis, were ran in a denaturing second dimension electrophoresis (2D-SDS PAGE). After collecting the first-dimension band and before the second dimension, first dimension bands were incubated in an Invitrogen™ Bolt™ MOPS SDS Running Buffer (Fisher Scientific) supplemented with β-mercaptoethanol (1% v/v) for 30min at RT. Acrylamide gradient Bolt™ 4-12% Bis-Tris Plus Gels (Thermo Scientific) were used for 2D SDS-PAGE, the gels were transferred and immunodetection was performed as previously described for classical SDS-PAGE. Immunoreactive bands were recorded by fluorescence and chemiluminescence with an Amersham ImageQuant 800. The FIJI software was used to quantify the perform densitometry analyses of images obtained.

Oxaloacetate quantification

Oxaloacetate level was measured using enzymatic assay based on citrate synthase activity. Intact heart (200µg) and liver (1000µg) mitochondria were incubated like for oxygen consumption measurement in an Oxygraph-2k at 37°C. Briefly, 150 µl of mitochondria incubated in 2.1 ml RB consuming oxygen under uncoupled condition were collected and quenched with 50µl ice cold acidic perchloric acid (PCA 7% without EDTA). Samples were then centrifuged 10 minutes at 30,000g and supernatants were quickly neutralized with KOMO (KOH (2 M); MOPS (0.5 M)). OAA content was then quantified using citrate synthase buffer (Acetyl-CoA (200 µM), 5,5'-dithiobis-(2-nitrobenzoic acid) (200 µM), Citrate Synthase from pig heart (4 U/ml) in phosphate buffer (50 mM, pH 7.2). Absorbance was recorded at 412 nm in UV Greiner bio-one 96-well plate by a CLARIOstar plate reader (BMG Labtech). Standard curve allowing OAA quantification was determined using fresh OAA solution.

NADH oxidation flux measurement ($JNAD^+$)

NAD^+ production rate was measured using enzymatic assay using G6PDH from *leuconostoc mesenteroides.* permeabilized mitochondria from heart (50 µg) and liver (100 µg) were incubated in 2.1 ml RB in an Oxygraph-2k at 37°C. 150 µl of mitochondria incubated in 2.1 ml RB buffer consuming oxygen under uncoupled condition were collected and quenched with 50µl ice cold acidic perchloric acid (PCA 7% without EDTA). Samples were then centrifuged 10 minutes at 30,000g and supernatants were quickly neutralized with KOMO (KOH (2 M); MOPS (0.5 M)). Neutralized samples were then subjected to enzymatic assay quantifying NAD^+ content as described previously (Bunoust et al., 2005).

Fumarate and Malate metabolic flux measurement

Metabolic fluxes were measured by ^{1}H-1D NMR. Intact Heart mitochondria were incubated in the same conditions than oxygen consumption measurements in an Oxygraph-2k at 37°C. During steady state respiration assessed under uncoupled conditions, aliquots collected at 0, 5, 7.5, and 12.5 minutes of incubation were snap frozen in liquid nitrogen to quench biochemical reactions. Metabolites were extracted with a mix of acetonitrile (ACN) and methanol (MeOH) to a final ACN/MeOH/Water proportion of 2:2:1. They were then vortexed, incubated at -20C for 20 min, and evaporated with a ThermoFisher SpeedVac SC250EXP concentrator. Samples were then dissolved into 200µL D_2O solution containing 2 mM Trimethyl-sillyl-propionic acid d4 (TSPd4) used as NMR reference standard, and centrifuged to remove membrane debris. A final 180 µL volume of the resulting supernatants were transferred into 3 mm NMR tubes. Samples were analyzed by 1H-1D NMR on a Bruker Ascend 800 MHz NMR spectrometer equipped with a 5 mm QPCI cryoprobe. A quantitative zgpr30 sequence was used with 64k acquisition points during 128 scans. The total repetition time between scans was set to 7 seconds. Malate and fumarate concentrations were quantified from their respective signals in the 1H-1D NMR spectra using TSPd4 as internal standard. All measurements were performed in triplicates.

Statistical analyses

Data are presented as mean ± SEM unless otherwise indicated in figure legends. Sample number (n) indicates the number of independent biological samples (individual mice) for each experiment. Sample numbers and experimental repeats are indicated in the figures. Data were analyzed with the GraphPad Prism software using unpaired Student's t- test, one-way ANOVA using Turkey's multiple comparison test, or two-way ANOVA using Bonferroni multiple comparison test between group comparison, as appropriate. A 0.05 p-value was considered statistically significant.

ACKNOWLEDGEMENTS

We gratefully acknowledge for the support, encouragement and useful discussions provided by Dr. Manuel Rojo. We would like to thank Prof. Michel Rigoulet and Prof. Nils-Göran Larsson, Dr. Dusanka Milenkovic for their precious feedback on the manuscript. We also thank Benoit Rousseau and Julien Izotte for the work at animal house (the service commun des animaleries, Animalerie A2 – University of Bordeaux). This work was supported by the AFM-Telethon Trampoline (AFM- 19613) and ANR (ANR-16-CE14-0013). The funders had no role in study design, data collection and analysis, decision to publish, or preparation of the manuscript. MetaboHub-MetaToul (Metabolomics & Fluxomics facilities, Toulouse, France, http://www.metatoul.fr) is supported by the ANR grant MetaboHUB-ANR-11-INBS-0010. JCP is grateful to INSERM for funding a temporary full-time researcher position.

DECLARATION OF INTERESTS

Authors declare no conflict of interest.

FIGURE LEGENDS

Figure 1: Heart and liver respiratory chain composition and bioenergetics.

(A, B) Oxygen consumption of intact heart (A) and liver (B) mitochondria assessed in presence of mitochondrial complex I substrates (PGM : pyruvate 10 mM, glutamate 5 mM, malate 5 mM), or complex II substrate (Succ+Rot : Succinate 10 mM and rotenone 30 nM), and PGM and succinate (Succ+PGM). Respiration are assessed under phosphorylating conditions (ADP+Pi), non-phosphorylating conditions (oligomycin), and uncoupled (CCCP titration). Heart (n= 15), liver (n= 5), error bars represent the mean ± SEM.

(C, D) Oxygen consumption of permeabilised heart (C) and liver (D) mitochondria assessed in presence of NADH (1.2 mM), Succinate (10 mM) and cytochrome *c* (62.5 µg/ml). Heart (n= 10), liver (n= 12), Error bars represent the mean ± SEM

(E) Mitochondrial cytochrome quantified from redox absorbance spectra. Cytochromes content of RC complexes: complex III (*b*, *c1*), complex IV (*a*, *a3*) and cytochrome *c* were determined in mitochondrial extracts of heart and liver. Heart (n= 6) liver (n= 6), error bars represent the mean ± SEM.

(F) Steady-state levels of OXPHOS subunits, in heart and liver mitochondria, determined by western blot analyses. Short and long exposure are performed to detect complex I (complex I *se* and complex I *le*) in the liver. Representative Western-blot of five different experiments.

(G) Relative amount of OXPHOS complexes (complex I– complex V) in heart and liver mitochondria determine by densitometric quantification of western blot experiments presented in (F), and normalized to heart OXPHOS complexes. (n= 5) Error bars represent the mean ± SEM

(H) Relative amount of complex I normalized to complex II in heart and liver mitochondria determined by densitometric analyses, (n= 5) Error bars represent the mean ± SEM.

Figure 2: Heart and liver respiratory chain supramolecular organization and preferential electron fuelling.

(A, B) Oxygen consumption of permeabilised mitochondria isolated from heart (A) and liver (B) assessed in presence of cytochrome *c* (62.5 µg/ml), complex I substrate NADH (1.2 mM), complex II substrate succinate (Succ, 10 mM) or both substrates simultaneously added. Addition of complex I (rotenone, 30 nM) or complex II (atpeninA5, 20 nM) specific inhibitor is used to discriminate complex I driven respiration (yellow) and complex II driven respiration (blue) when mitochondria are incubated with NADH and succinate. Heart (n= 9), Liver (n= 12), error bars represent the mean ± SEM

(C, D) complex I driven NAD^+ synthesis flux assessed in permeabilised mitochondria isolated from heart (C) and liver (D), incubated in presence of cytochrome *c* (62.5 µg/ml), complex I substrate NADH (1.2 mM) and/or complex II substrate succinate (Succ, 10 mM). Heart (n=6), liver (n= 9), error bars represent the mean ± SEM.

(E, F) Supramolecular organisation of heart and liver RC. Heart and liver mitochondria are solubilized with a digitonin/protein ratio of 3:1 (g/g) and RC are resolved with 4-16% (E) or 3-12% (F) BN-PAGE, followed by complex I-, complex II- and complex IV-IGA assays, or by western blot using antibody toward ND1, SDHC, UQCRC2 or COX1 subunits. Representative of three different experiments. Heart (n= 3), liver (n= 3).

(G, H) RC complexes composition of heart (G) and liver (H). Supramolecular organisation of RC is assessed by 2D-BN/SDS-PAGE and immunoblot analyses are performed with OXPHOS cocktail antibodies toward NDUFB8, MTCO1, UQCR2 and ATP5A subunits. Densitometric profile of complex I (black), complex III (green) and complex IV (orange) detected by immunoblot are represented on top of Coomassie staining. Representative of three different experiments. Heart (n= 3), liver (n= 3).

(I) Relative amount of complex I, complex II, complex III and complex IV associated in respirasome (complex I-III-IV) or in supercomplexes containing complex I (complex I_x-III_y or complex I_x-IV_y) in heart (red bars) and liver (green bars). Proportion of complexes found associated in respirasome is determined by densitometric quantification of 2D-BN/SDS-PAGE. Heart (n= 3), Liver (n= 3), Error bars represent the mean ± SEM.

Figure 3: Internal OAA level orchestrates the respective contribution of complex I and II to feed the respiratory chain with electrons

(A, B) Oxygen consumption of uncoupled heart (A) and liver (B) intact mitochondria assessed in presence of complex I substrates (PGM) and/or complex II substrate (Succ). Addition of complex I (rotenone, 30 nM) or complex II (atpeninA5, 20 nM) specific inhibitor is used to discriminate complex I dependent respiration (yellow bars) and complex II dependent respiration (blue bars) when mitochondria are incubated with PGM and Succ. Heart (n= 17), liver (n= 6), error bars represent the mean ± SEM.

(C, D) Oxaloacetate levels assessed when uncoupled heart (C) and liver (D) intact mitochondria are fed with complex I substrates (PGM) and/or complex II substrate (Succ). Heart (n= 4), Liver (n= 3), Error bars represent the mean ± SEM.

(E) Mitochondrial NAD(P)H fluorescence of uncoupled heart mitochondria incubated with complex I substrates (PGM) ± rotenone (30 nM), or complex II substrate (Succ) ± rotenone (30 nM), or both (Succ+PGM). (n= 5), error bars represent the mean ± SEM.

(F) 1H-1D NMR quantification of fumarate (circle) and malate (scare) content are assessed in uncoupled heart mitochondria oxidizing succinate in absence (blue) or in presence of rotenone (30 nM) (red). (n= 3), error bars represent the mean ± SEM.

Figure 4: MDH2 rewires TCA cycle and respiratory chain electron flows to favour NADH oxidation

Scheme of respiratory chain, TCA cycle (blue background), and malate-aspartate shuttle (MAS, red background) enlightening the key metabolic role played by MDH2.

(B, C) Oxygen consumption (B) and oxaloacetate level (C) assessed with intact heart mitochondria fed with succinate and increased concentration of malate during uncoupled respiration. (n= 4), error bars represent the mean ± SEM.

(D) Correlation between mitochondrial oxygen consumption and oxaloacetate levels of intact heart mitochondria isolated fed with succinate and increased concentration of malate. Error bars represent the mean ± SEM.

(E) Oxaloacetate levels assessed with intact heart mitochondria in presence of different substrates condition metabolizing endogenously produced OAA (Succ+Glu, Succ+Pyr, Succ+PG). (n= 4), error bars represent the mean ± SEM.

(F) Oxygen consumption of intact heart mitochondria fed with indicated substrates (Succ+Glu, Succ+Pyr, Succ+PG). Addition of specific inhibitor of complex I (rotenone, 30nM) and complex II (AtpeninA5, 20nM) during uncoupled respiration, determine the complex I driven respiration (yellow bars) or complex II driven respiration (blue bars). (n= 8), error bars represent the mean ± SEM.

(G) Correlation between oxygen consumption of intact heart mitochondria fed with succinate, pyruvate, glutamate and increasing concentration of malate. Complex I driven (yellow circle) or complex II driven (blue circle) respiration are determined through sequential addition of specific complex I (rotenone, 30nM) and complex II (AtpeninA5, 20nM) inhibitors. (n= 4), error bars represent the mean ± SEM.

Figure 1S: Complex I and complex II driven respiration depend strongly of substrate combination.

(A, B) Oxygen consumption of intact mitochondria isolated from heart were assessed in presence of unique (A) or mixed combination of substrates (B) which mitochondrial metabolism result in delivering NADH to complex I (pyruvate 10 mM, glutamate 5 mM, malate 5 mM). Respiration are assessed under phosphorylating conditions (ADP+Pi), non-phosphorylating conditions (oligomycin), and uncoupled (CCCP titration). (n= 4) Error bars represent the mean ± SEM

(C, D) Oxygen consumption of intact mitochondria isolated from heart (C) and liver (D) are assessed in presence of succinate ± rotenone (30 nM) under phosphorylating conditions (ADP+Pi), non-phosphorylating conditions (oligomycin), and uncoupled (CCCP titration). Heart (n= 28), Liver (n= 11), Error bars represent the mean ± SEM

Figure 2S: Heart and liver mitochondrial respiratory chain's enzymes stoichiometry, supramolecular organization and preferential electron fuelling.

(A-D) Oxygen consumption of uncoupled heart (A, B) and liver (C, D) intact mitochondria in presence of mitochondrial complex I substrates (PGM, yellow bars) (A, C), or complex II substrate (Succ, blue bars) (B,D). Complex I (A, C) or complex II (B, D) driven respiration are recorded ± rotenone (rot, complex I inhibitor, 30 nM), or Atpenin A5 (AtpnA5, complex II inhibitor, 20 nM). Heart (n= 5), liver (n= 5), Error bars represent the mean ± SEM.

(E) Supramolecular organisation of heart and liver respiratory chain. Heart and liver mitochondria are solubilized with a digitonin/protein ratio of 3:1 (g/g) and high MW assemblies are resolved using 4-16% BN-PAGE, followed by complex I-, complex II- and complex IV-IGA assays, or by western blot analyses using antibody against ND1, SDHC, UQCRC2 or COX1 subunits. Representative of three different experiments. Heart (n= 3), liver (n= 3).

(F, G) RC complexes composition of heart (F) and liver (G) SC assessed by 2D-BN/SDS-PAGE and immunoblot analyses are performed with OXPHOS cocktail antibodies against NDUFB8, MTCO1, UQCR2 and ATP5A subunits. Heart (n= 3), liver (n= 3).

(H, I) Supramolecular organisation of heart respiratory chain incubated with different respiratory substrate. Heart and liver mitochondria incubated with PGM, succinate ± rotenone (Succ, Succ+rot), succinate glutamate (Succ+Glu) or succinate pyruvate and glutamate (Succ+PG) are solubilized with a digitonin/protein ratio of 3:1 (g/g) and RC are resolved with 3-12% (H) or 4-16% (I) BN-PAGE , followed by complex I-, complex II- and complex IV-IGA assays. Representative of three different experiments. Heart (n= 3).

Figure 3S: Internal OAA level orchestrates the respective contribution of complex I and II to feed the respiratory chain with electrons

(A) Oxygen consumption of permeabilised heart mitochondria in presence of cytochrome *c* (62.5 µg/ml), and increasing concentration of oxaloacetate are added when mitochondria are incubated with NADH (yellow bars) or with succinate (blue bars). (n=3), error bars represent the mean ± SEM.

(B) NAD(P)H fluorescence of uncoupled liver mitochondria incubated with complex I substrates (PGM) ± rotenone (30 nM), or complex II substrate (Succ) ± rotenone (30 nM), or both (Succ+PGM). Liver (n= 3), error bars represent the mean ± SEM.

(C,D) Oxygen consumption of uncoupled heart (C) and liver (D) intact mitochondria fed with complex I substrates (PGM) and/or complex II substrate (Succ). Addition of complex I (rotenone, 30 nM) or complex II (atpeninA5, 20 nM) specific inhibitor are used to discriminate complex I dependent respiration (yellow bars) and complex II dependent respiration (blue bars) when mitochondria are incubated with both PGM and succinate. Complex I and complex II inhibitor were added sequentially (sequence addition are indicated in the table below the graph:

1st for firstly added and 2nd for the one added after). Heart (n= 11), liver (n= 4), error bars represent the mean ± SEM.

Figure 4S: MDH2 rewires TCA cycle and respiratory chain electrons flow to favour NADH oxidation

(A, B) Oxygen consumption (A) oxaloacetate level (C) assessed with intact liver mitochondria fed with succinate and increased concentration of malate during uncoupled respiration. (n= 3), error bars represent the mean ± SEM.

(C) Correlation between mitochondrial oxygen consumption and oxaloacetate levels of intact liver mitochondria isolated fed with succinate and increasing concentration of malate. Error bars represent the mean ± SEM.

(D) Oxygen consumption of permeabilised heart mitochondria fed with complex I (NADH, yellow bars) or complex II (Succ, blue bars) substrates ± addition of oxaloacetate (hatched bars) or malate (dotted bars). (n= 4), error bars represent the mean ± SEM.

(E) Oxygen consumption of uncoupled heart mitochondria fed with succinate (10mM) and malate (5 mM). Addition of complex I (rotenone, 30 nM) or complex II (atpeninA5, 20 nM) specific inhibitor are used to quantify the complex I driven respiration (yellow bars) and complex II driven respiration (blue bars). Complex I and complex II inhibitor were added sequentially (sequence addition are mentioned in the table below the graph). (n= 5), error bars represent the mean ± SEM.

(F) Oxaloacetate levels assessed with intact liver mitochondria in presence of different substrates condition metabolizing endogenously produced OAA (Succ+Glu, Succ+Pyr, Succ+PG). (n= 3), error bars represent the mean ± SEM.

(G) Oxygen consumption of intact liver mitochondria fed with indicated substrates conditions (Succ+Pyr, Succ+Glu or Succ+Pyr+Glu). Addition of specific inhibitor of complex I (rotenone) and complex II (AtpeninA5) during uncoupled respiration, determine the complex I driven respiration (yellow bars) or complex II driven respiration (blue bars). (n= 5), error bars represent the mean ± SEM.

REFERENCES

Acín-Pérez, R., Fernández-Silva, P., Peleato, M.L., Pérez-Martos, A., and Enriquez, J.A. (2008). Respiratory Active Mitochondrial Supercomplexes. Mol. Cell *32*, 529–539.

Alkan, H.F., Vesely, P.W., Hackl, H., Foßelteder, J., Schmidt, D.R., Vander Heiden, M.G., Pichler, M., Hoefler, G., and Bogner-Strauss, J.G. (2020). Deficiency of malate-aspartate shuttle component SLC25A12 induces pulmonary metastasis. Cancer Metab. *8*, 26.

Balsa, E., Soustek, M.S., Thomas, A., Cogliati, S., García-Poyatos, C., Martín-García, E., Jedrychowski, M., Gygi, S.P., Enriquez, J.A., and Puigserver, P. (2019). ER and Nutrient Stress Promote Assembly of Respiratory Chain Supercomplexes through the PERK-eIF2α Axis. Mol. Cell *74*, 877-890.e6.

Bianchi, C., Genova, M.L., Parenti Castelli, G., and Lenaz, G. (2004). The mitochondrial respiratory chain is partially organized in a supercomplex assembly: kinetic evidence using flux control analysis. J. Biol. Chem. *279*, 36562–36569.

Blaza, J.N., Serreli, R., Jones, A.J.Y., Mohammed, K., and Hirst, J. (2014). Kinetic evidence against partitioning of the ubiquinone pool and the catalytic relevance of respiratory-chain supercomplexes. Proc. Natl. Acad. Sci. U. S. A. *111*, 15735–15740.

Borst, P. (2020). The malate–aspartate shuttle (Borst cycle): How it started and developed into a major metabolic pathway. IUBMB Life *72*, 2241–2259.

Brandt, T., Mourier, A., Tain, L.S., Partridge, L., Larsson, N.-G., and Kühlbrandt, W. (2017). Changes of mitochondrial ultrastructure and function during ageing in mice and Drosophila. ELife *6*, e24662.

Bunoust, O., Devin, A., Avéret, N., Camougrand, N., and Rigoulet, M. (2005). Competition of Electrons to Enter the Respiratory Chain: a new regulatory mechanism of oxidative metabolism in saccharomyces cerevisiae. J. Biol. Chem. *280*, 3407–3413.

Cederbaum, A.I., Lieber, C.S., Beattie, D.S., and Rubin, E. (1973). Characterization of shuttle mechanisms for the transport of reducing equivalents into mitochondria. Arch. Biochem. Biophys. *158*, 763–781.

Chance, B., and Williams, G.R. (1956). The Respiratory Chain and Oxidative Phosphorylation. In Advances in Enzymology and Related Areas of Molecular Biology, (John Wiley & Sons, Ltd), pp. 65–134.

Chavez, J.D., Lee, C.F., Caudal, A., Keller, A., Tian, R., and Bruce, J.E. (2018). Chemical Crosslinking Mass Spectrometry Analysis of Protein Conformations and Supercomplexes in Heart Tissue. Cell Syst. *6*, 136-141.e5.

Davies, K.M., Blum, T.B., and Kühlbrandt, W. (2018). Conserved in situ arrangement of complex I and III2 in mitochondrial respiratory chain supercomplexes of mammals, yeast, and plants. Proc. Natl. Acad. Sci. U. S. A. *115*, 3024–3029.

Dawson, A.G. (1979). Oxidation of cytosolic NADH formed during aerobic metabolism in mammalian cells. Trends Biochem. Sci. *4*, 171–176.

Devin, A., Bouchez, C., Molinié, T., David, C., Duvezin-Caubet, S., Rojo, M., Mourier, A., Averet, N., and Rigoulet, M. (2019). Chapter 1 - Mitochondria: Ultrastructure, Dynamics, Biogenesis and Main Functions. In Mitochondria in Obesity and Type 2 Diabetes, B. Morio, L. Pénicaud, and M. Rigoulet, eds. (Academic Press), pp. 3–32.

Dudkina, N.V., Kouřil, R., Peters, K., Braun, H.-P., and Boekema, E.J. (2010). Structure and

function of mitochondrial supercomplexes. Biochim. Biophys. Acta BBA - Bioenerg. *1797*, 664–670.

Enríquez, J.A. (2016). Supramolecular Organization of Respiratory Complexes. Annu. Rev. Physiol. *78*, 533–561.

Fedor, J.G., and Hirst, J. (2018). Mitochondrial Supercomplexes Do Not Enhance Catalysis by Quinone Channeling. Cell Metab. *28*, 525-531.e4.

Fink, B.D., Bai, F., Yu, L., Sheldon, R.D., Sharma, A., Taylor, E.B., and Sivitz, W.I. (2018). Oxaloacetic acid mediates ADP-dependent inhibition of mitochondrial complex II-driven respiration. J. Biol. Chem. *293*, 19932–19941.

Gnaiger, E. (2009). Capacity of oxidative phosphorylation in human skeletal muscle: New perspectives of mitochondrial physiology. Int. J. Biochem. Cell Biol. *41*, 1837–1845.

Greggio, C., Jha, P., Kulkarni, S.S., Lagarrigue, S., Broskey, N.T., Boutant, M., Wang, X., Conde Alonso, S., Ofori, E., Auwerx, J., et al. (2017). Enhanced Respiratory Chain Supercomplex Formation in Response to Exercise in Human Skeletal Muscle. Cell Metab. *25*, 301–311.

Gu, J., Wu, M., Guo, R., Yan, K., Lei, J., Gao, N., and Yang, M. (2016). The architecture of the mammalian respirasome. Nature *537*, 639–643.

Kohl, J.B., Mellis, A.-T., and Schwarz, G. (2019). Homeostatic impact of sulfite and hydrogen sulfide on cysteine catabolism. Br. J. Pharmacol. *176*, 554–570.

Laemmli, U.K. (1970). Cleavage of Structural Proteins during the Assembly of the Head of Bacteriophage T4. Nature *227*, 680–685.

LaNoue, K.F., Wałajtys, E.I., and Williamson, J.R. (1973). Regulation of Glutamate Metabolism and Interactions with the Citric Acid Cycle in Rat Heart Mitochondria. J. Biol. Chem. *248*, 7171–7183.

LaNoue, K.F., Meijer, A.J., and Brouwer, A. (1974). Evidence for electrogenic aspartate transport in rat liver mitochondria. Arch. Biochem. Biophys. *161*, 544–550.

Lapuente-Brun, E., Moreno-Loshuertos, R., Acín-Pérez, R., Latorre-Pellicer, A., Colás, C., Balsa, E., Perales-Clemente, E., Quirós, P.M., Calvo, E., Rodríguez-Hernández, M.A., et al. (2013). Supercomplex Assembly Determines Electron Flux in the Mitochondrial Electron Transport Chain. Science *340*, 1567–1570.

Lee, W.-C., Ji, X., Nissim, I., and Long, F. (2020). Malic Enzyme Couples Mitochondria with Aerobic Glycolysis in Osteoblasts. Cell Rep. *32*, 108108.

Letts, J.A., Fiedorczuk, K., and Sazanov, L.A. (2016). The architecture of respiratory supercomplexes. Nature *537*, 644–648.

Mitchell, P. (1961). Coupling of phosphorylation to electron and hydrogen transfer by a chemi-osmotic type of mechanism. Nature *191*, 144–148.

Mourier, A., Devin, A., and Rigoulet, M. (2010). Active proton leak in mitochondria: a new way to regulate substrate oxidation. Biochim. Biophys. Acta *1797*, 255–261.

Mourier, A., Matic, S., Ruzzenente, B., Larsson, N.-G., and Milenkovic, D. (2014). The Respiratory Chain Supercomplex Organization Is Independent of COX7a2l Isoforms. Cell Metab. *20*, 1069–1075.

Mourier, A., Motori, E., Brandt, T., Lagouge, M., Atanassov, I., Galinier, A., Rappl, G., Brodesser, S., Hultenby, K., Dieterich, C., et al. (2015). Mitofusin 2 is required to maintain

mitochondrial coenzyme Q levels. J Cell Biol *208*, 429–442.

Påhlman, I.-L., Gustafsson, L., Rigoulet, M., and Larsson, C. (2001). Cytosolic redox metabolism in aerobic chemostat cultures of Saccharomyces cerevisiae. Yeast *18*, 611–620.

Purvis, J.L., and Lowenstein, J.M. (1961). The Relation between Intra- and Extramitochondrial Pyridine Nucleotides. J. Biol. Chem. *236*, 2794–2803.

Rieger, B., Shalaeva, D.N., Söhnel, A.-C., Kohl, W., Duwe, P., Mulkidjanian, A.Y., and Busch, K.B. (2017). Lifetime imaging of GFP at CoxVIIIa reports respiratory supercomplex assembly in live cells. Sci. Rep. *7*, 46055.

Safer, B., Smith, C.M., and Williamson, J.R. (1971). Control of the transport of reducing equivalents across the mitochondrial membrane in perfused rat heart. J. Mol. Cell. Cardiol. *2*, 111–124.

Safer B (1975). The Metabolic Significance of the Malate-Aspartate Cycle in Heart. Circ. Res. *37*, 527–533.

Schägger, H., and Pfeiffer, K. (2000). Supercomplexes in the respiratory chains of yeast and mammalian mitochondria. EMBO J. *19*, 1777–1783.

Schägger, H., and Pfeiffer, K. (2001). The Ratio of Oxidative Phosphorylation Complexes I–V in Bovine Heart Mitochondria and the Composition of Respiratory Chain Supercomplexes*. J. Biol. Chem. *276*, 37861–37867.

Schollmeyer, P., and Klingenberg, M. (1961). Oxaloacetate and adenosinetriphosphate levels during inhibition and activation of succinate oxidation. Biochem. Biophys. Res. Commun. *4*, 43–47.

Trouillard, M., Meunier, B., and Rappaport, F. (2011). Questioning the functional relevance of mitochondrial supercomplexes by time-resolved analysis of the respiratory chain. Proc. Natl. Acad. Sci. *108*, E1027–E1034.

Wittig, I., Carrozzo, R., Santorelli, F.M., and Schägger, H. Functional assays in high-resolution clear native gels to quantify mitochondrial complexes in human biopsies and cell lines. ELECTROPHORESIS *28*, 3811–3820.

FIGURE 1

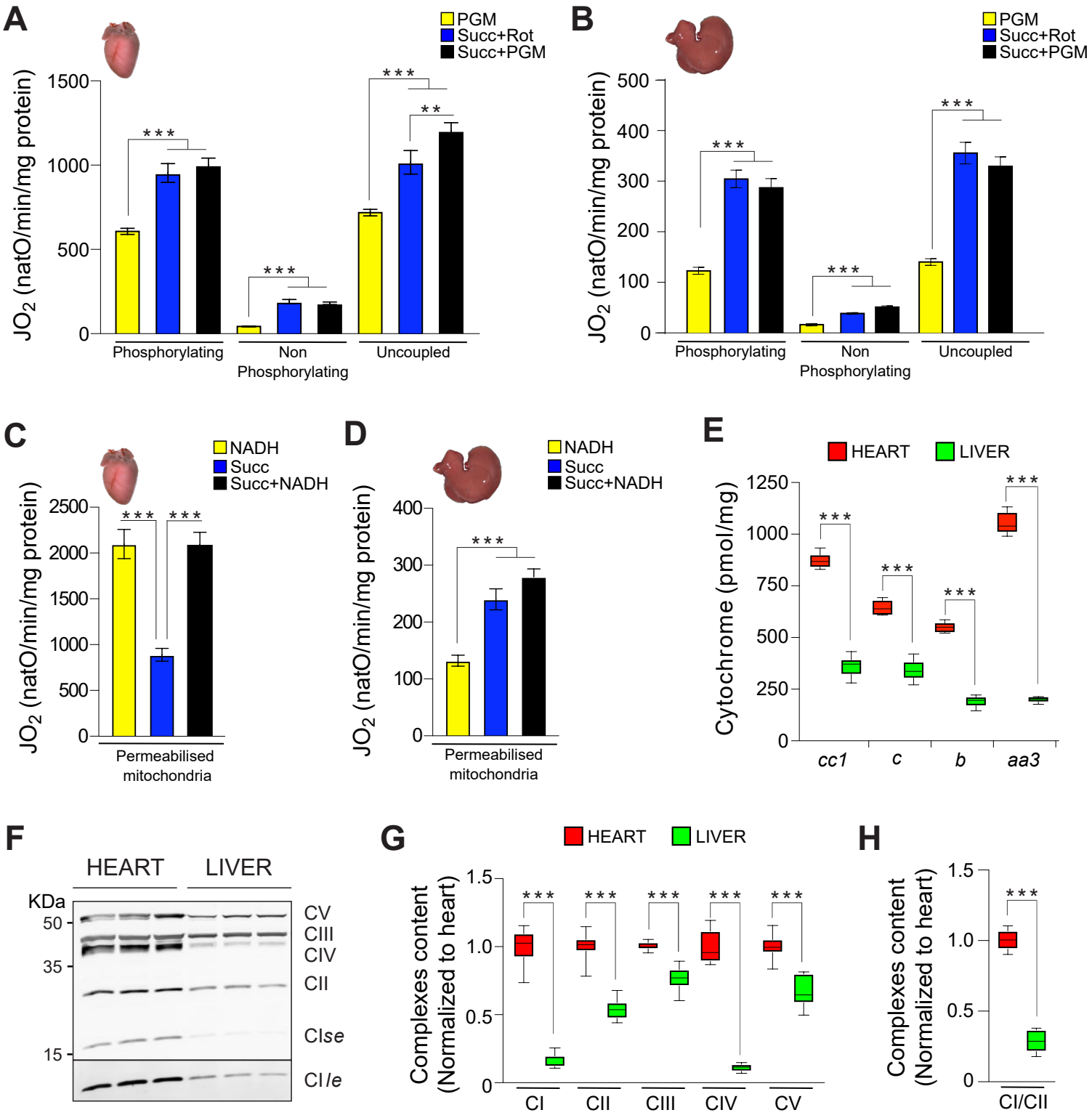

FIGURE 2

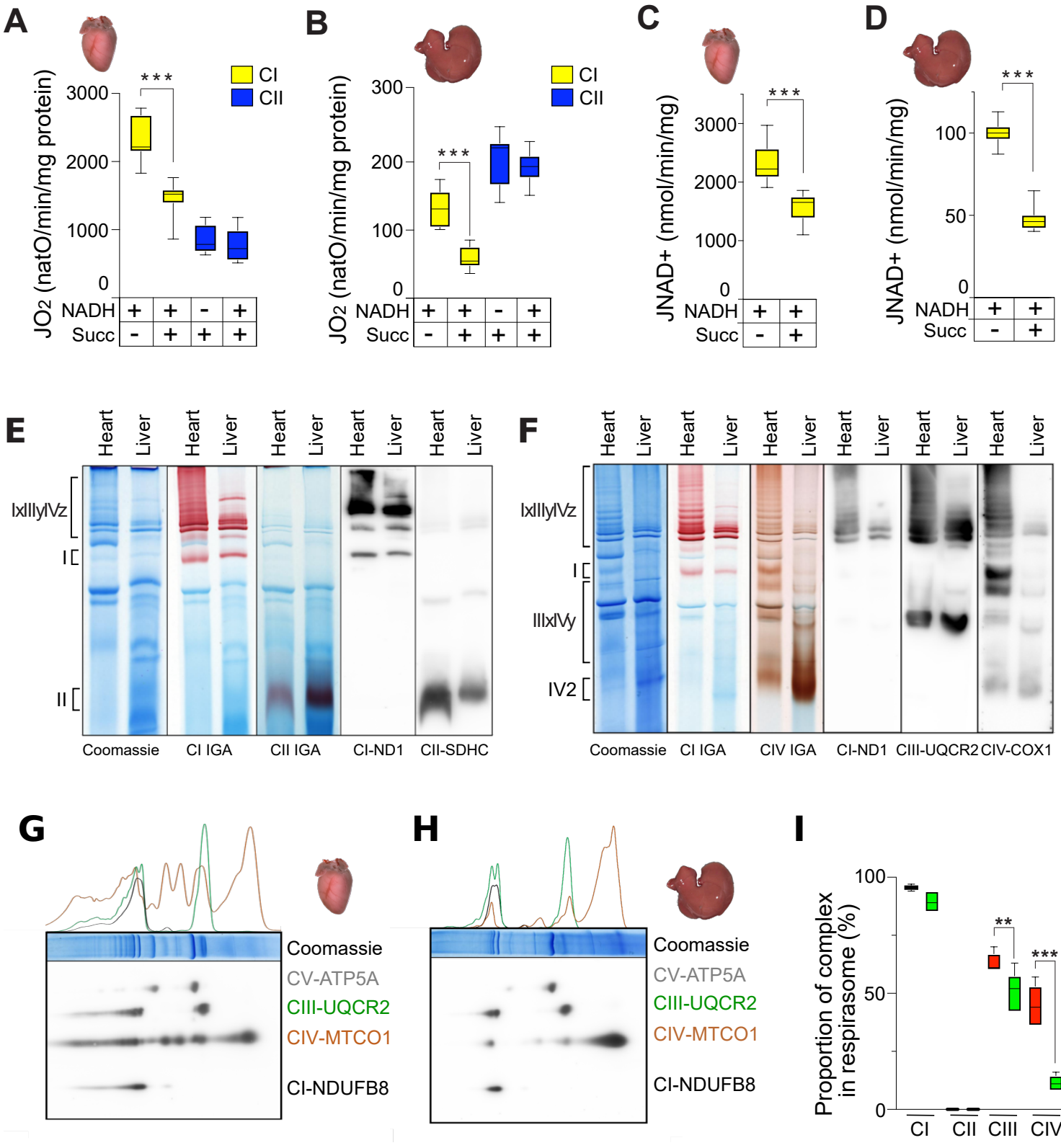

FIGURE 3

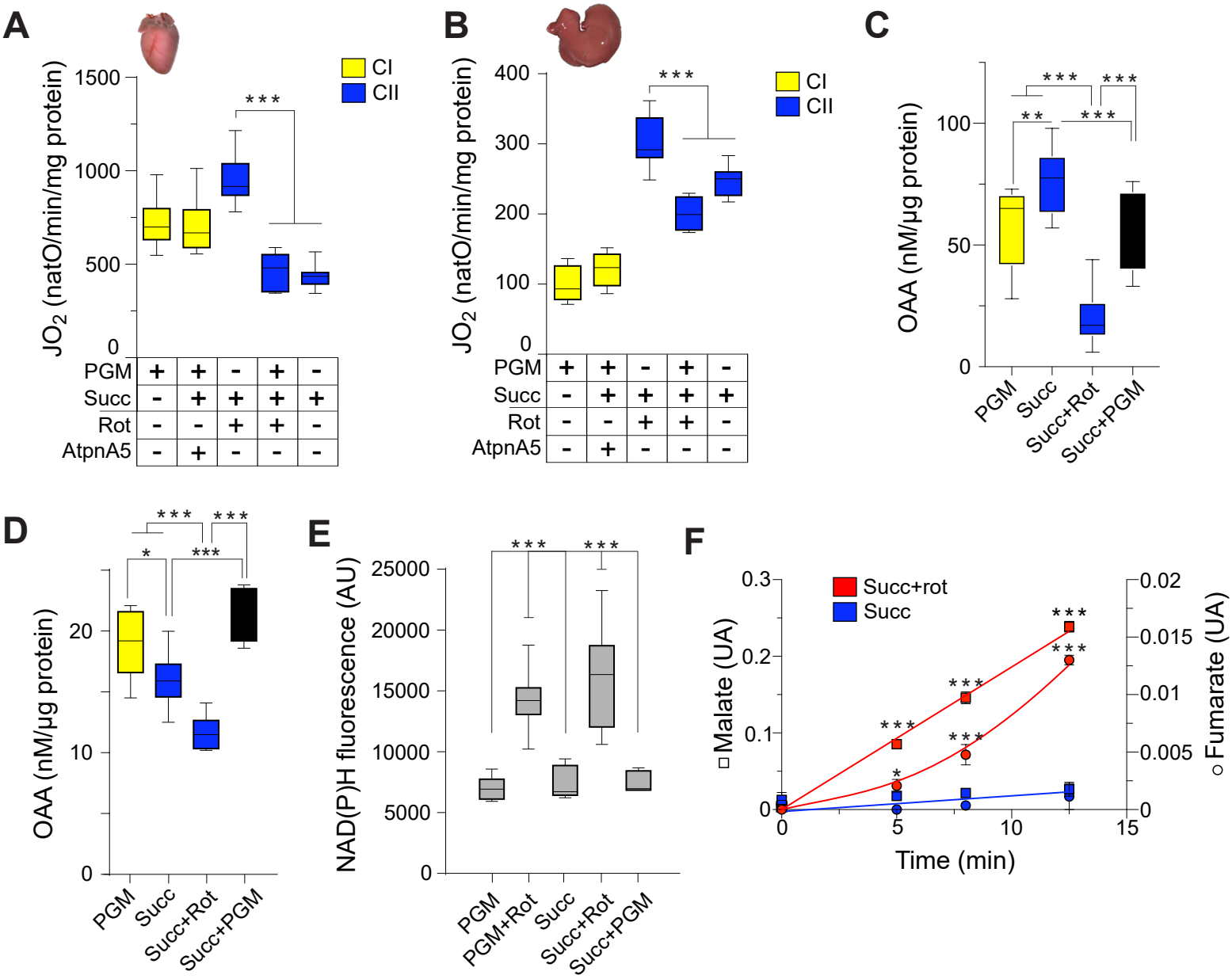

FIGURE 4

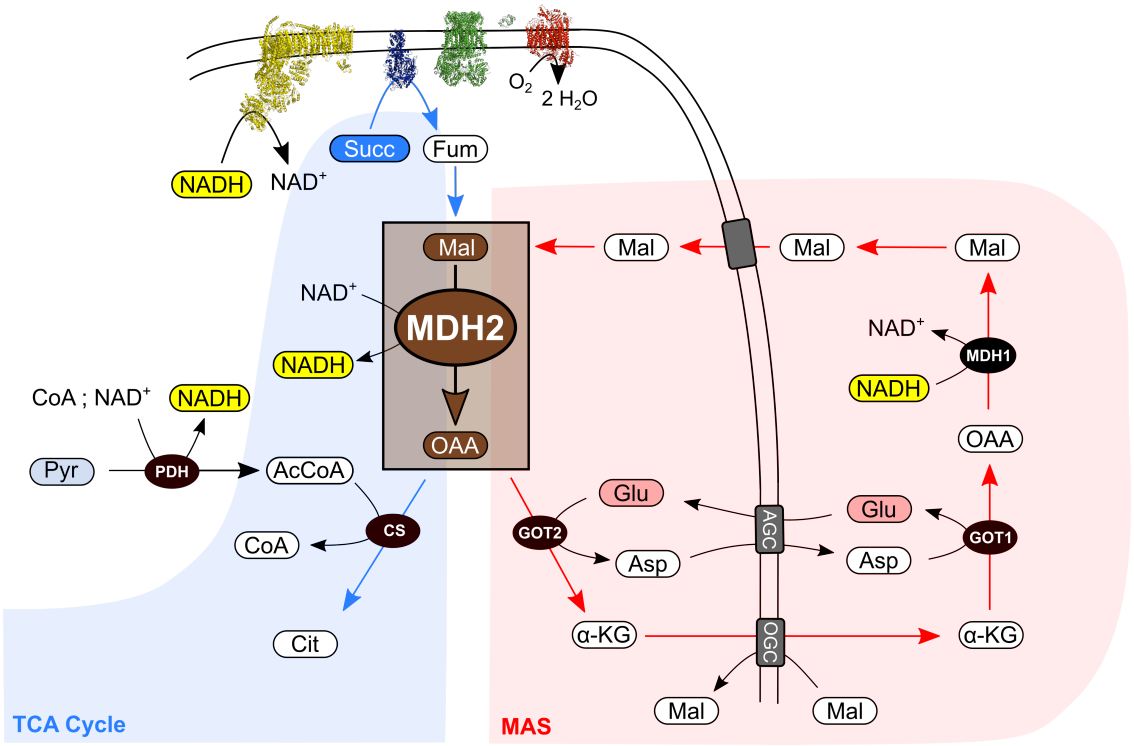

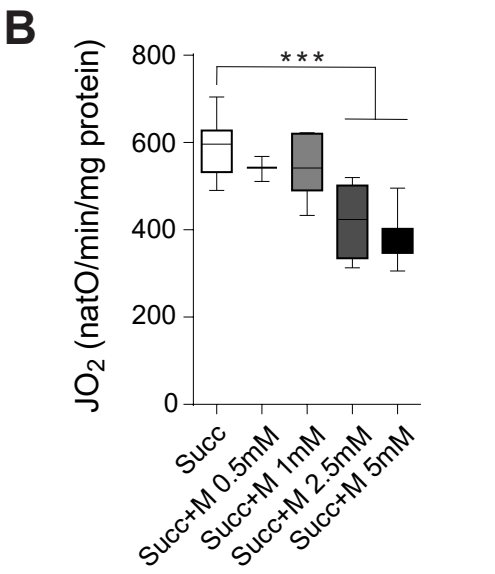

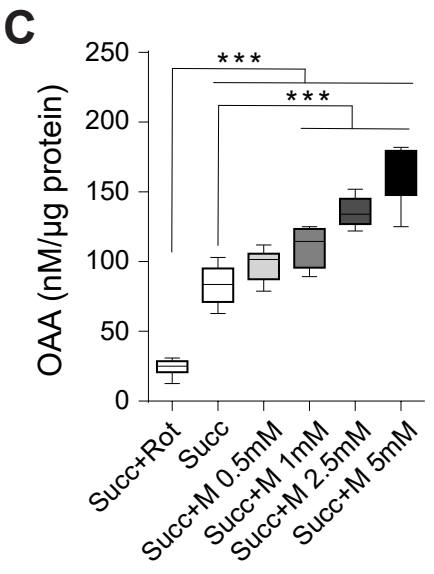

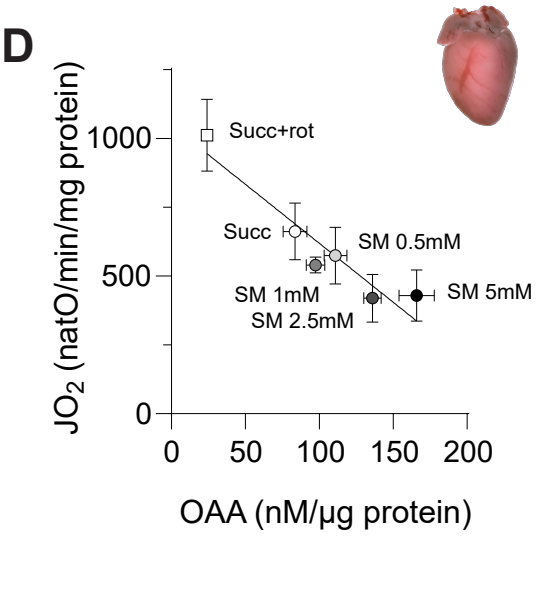

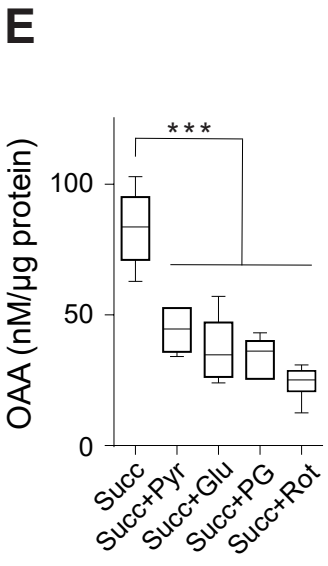

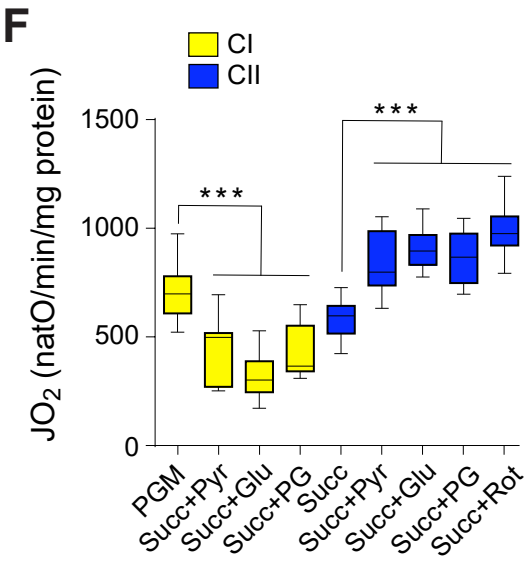

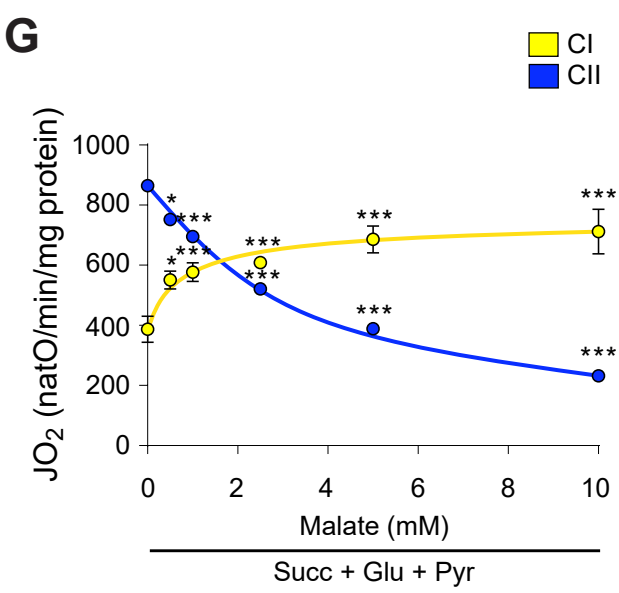

FIGURE S1

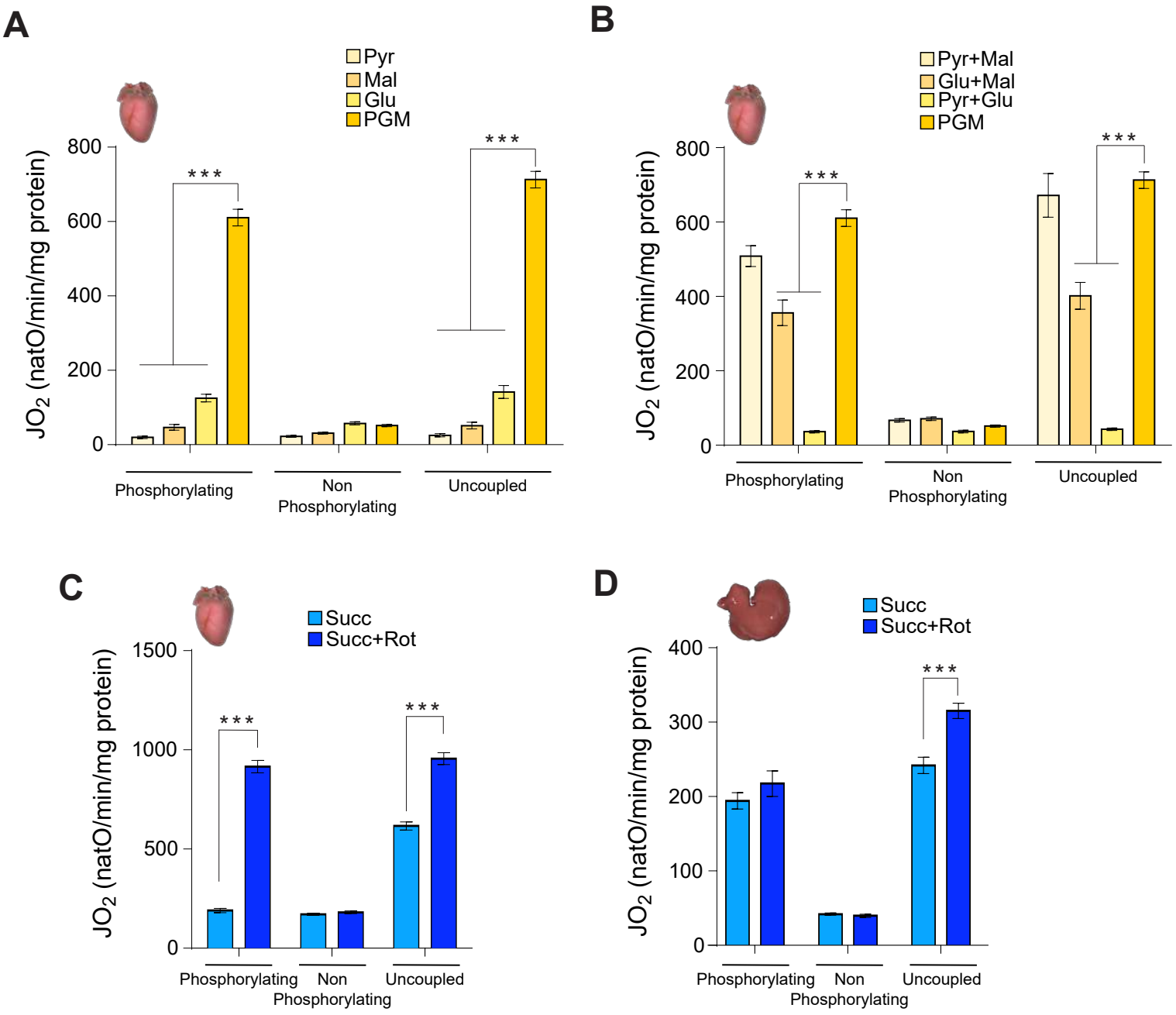

Figure 1S: Complex I and complex II driven respiration depend strongly of substrate combination

(A, B) Oxygen consumption of intact mitochondria isolated from heart were assessed in presence of unique (A) or mixed combination of substrates (B) which mitochondrial metabolism result in delivering NADH to complex I (pyruvate 10 mM, glutamate 5 mM, malate 5 mM). Respiration are assessed under phosphorylating conditions (ADP+Pi), non-phosphorylating conditions (oligomycin), and uncoupled (CCCP titration). (n= 4) Error bars represent the mean ± SEM

(C, D) Oxygen consumption of intact mitochondria isolated from heart (C) and liver (D) are assessed in presence of succinate ± rotenone (30 nM) under phosphorylating conditions (ADP+Pi), non-phosphorylating conditions (oligomycin), and uncoupled (CCCP titration). Heart (n= 28), Liver (n= 11), Error bars represent the mean ± SEM

Figure S2

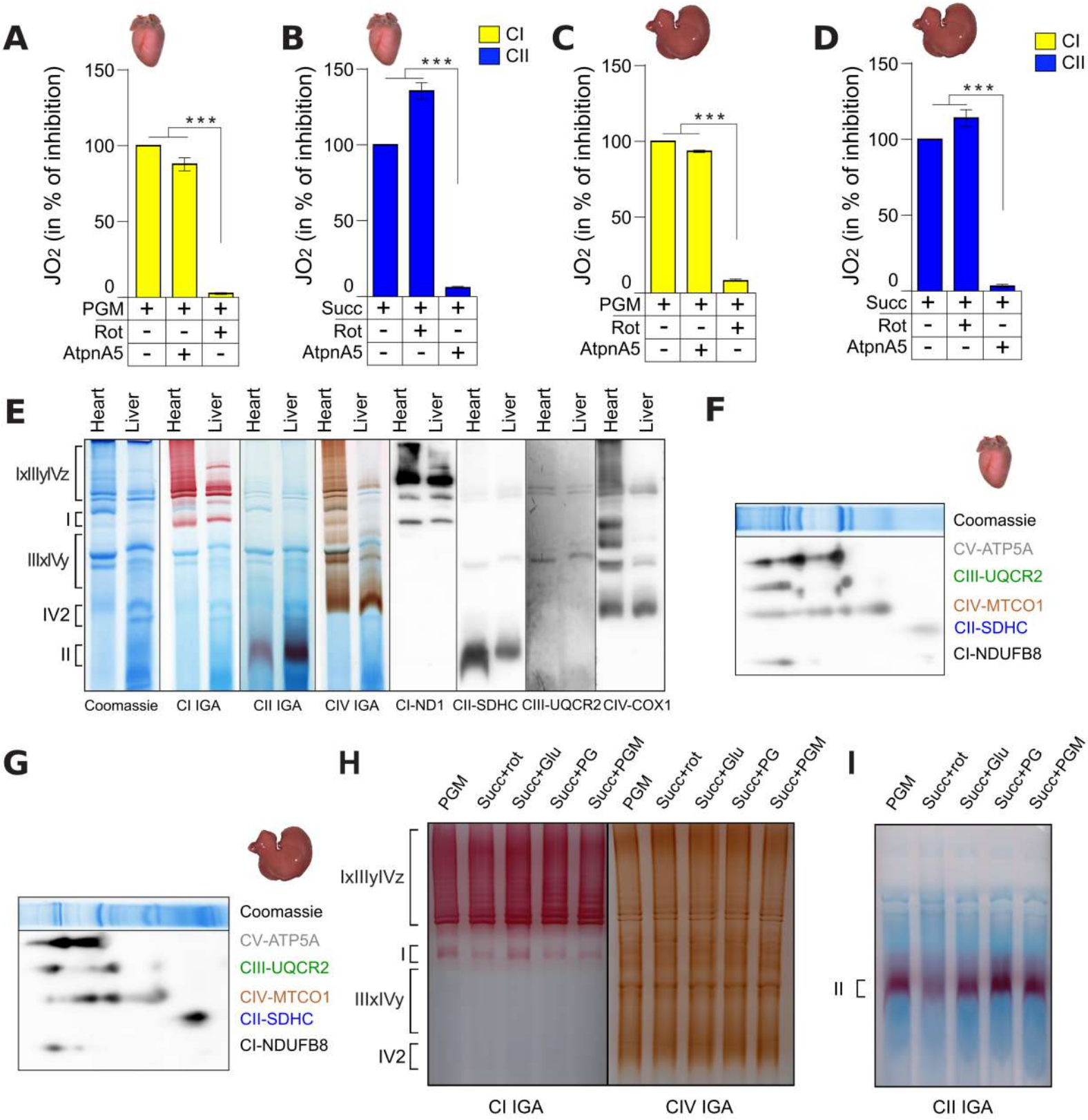

Figure 2S: Heart and liver mitochondrial respiratory chain's enzymes stoichiometry, supramolecular organization and preferential electron fuelling

(A-D) Oxygen consumption of uncoupled heart (A, B) and liver (C, D) intact mitochondria in presence of mitochondrial complex I substrates (PGM, yellow bars) (A, C), or complex II substrate (Succ, blue bars) (B,D). Complex I (A, C) or complex II (B, D) driven respiration are recorded ± rotenone (rot, complex I inhibitor, 30 nM), or Atpenin A5 (AtpnA5, complex II inhibitor, 20 nM). Heart (n= 5), liver (n= 5), Error bars represent the mean ± SEM.

(E) Supramolecular organisation of heart and liver respiratory chain. Heart and liver mitochondria are solubilized with a digitonin/protein ratio of 3:1 (g/g) and high MW assemblies are resolved using 4-16% BN-PAGE, followed by complex I-, complex II- and complex IV-IGA assays, or by western blot analyses using antibody against ND1, SDHC, UQCRC2 or COX1 subunits. Representative of three different experiments. Heart (n= 3), liver (n= 3).

(F, G) RC complexes composition of heart (F) and liver (G) SC assessed by 2D-BN/SDS-PAGE and immunoblot analyses are performed with OXPHOS cocktail antibodies against NDUFB8, MTCO1, UQCR2 and ATP5A subunits. Heart (n= 3), liver (n= 3).

(H, I) Supramolecular organisation of heart respiratory chain incubated with different respiratory substrate. Heart and liver mitochondria incubated with PGM, succinate ± rotenone (Succ, Succ+rot), succinate glutamate (Succ+Glu) or succinate pyruvate and glutamate (Succ+PG) are solubilized with a digitonin/protein ratio of 3:1 (g/g) and RC are resolved with 3-12% (H) or 4-16% (I) BN-PAGE , followed by complex I-, complex II- and complex IV-IGA assays. Representative of three different experiments. Heart (n= 3).

FIGURE S3

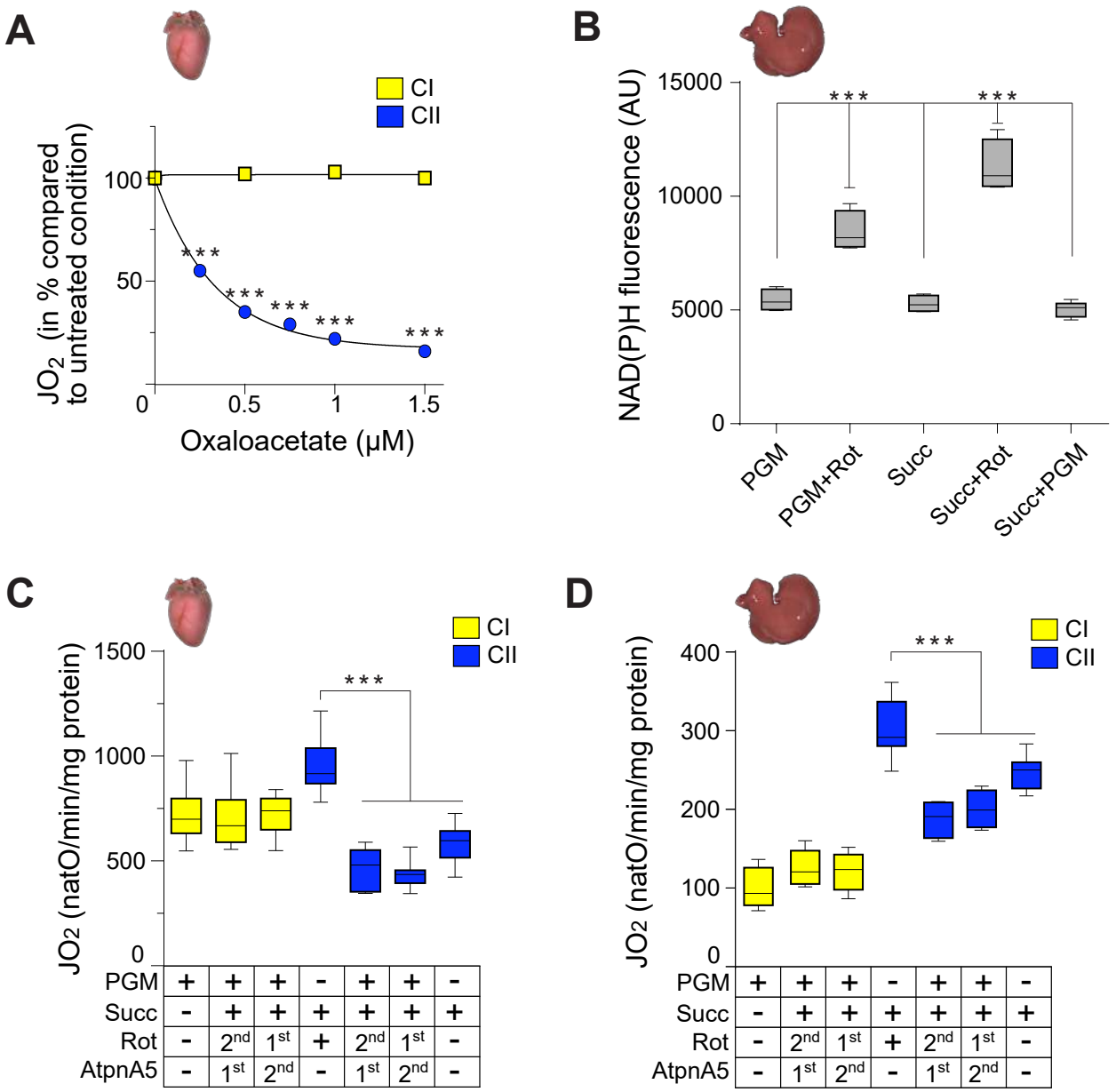

Figure 3S: Internal OAA level orchestrates the respective contribution of complex I and II to feed the respiratory chain with electrons

(A) Oxygen consumption of permeabilised heart mitochondria in presence of cytochrome *c* (62.5 µg/ml), and increasing concentration of oxaloacetate are added when mitochondria are incubated with NADH (yellow bars) or with succinate (blue bars). (n=3), error bars represent the mean ± SEM.

(B) NAD(P)H fluorescence of uncoupled liver mitochondria incubated with complex I substrates (PGM) ± rotenone (30 nM), or complex II substrate (Succ) ± rotenone (30 nM), or both (Succ+PGM). Liver (n= 3), error bars represent the mean ± SEM.

(C, D) Oxygen consumption of uncoupled heart (C) and liver (D) intact mitochondria fed with complex I substrates (PGM) and/or complex II substrate (Succ). Addition of complex I (rotenone, 30 nM) or complex II (atpeninA5, 20 nM) specific inhibitor are used to discriminate complex I dependent respiration (yellow bars) and complex II dependent respiration (blue bars) when mitochondria are incubated with both PGM and succinate. Complex I and complex II inhibitor were added sequentially (sequence addition are indicated in the table below the graph: 1st for firstly added and 2nd for the one added after). Heart (n= 11), liver (n= 4), error bars represent the mean ± SEM.

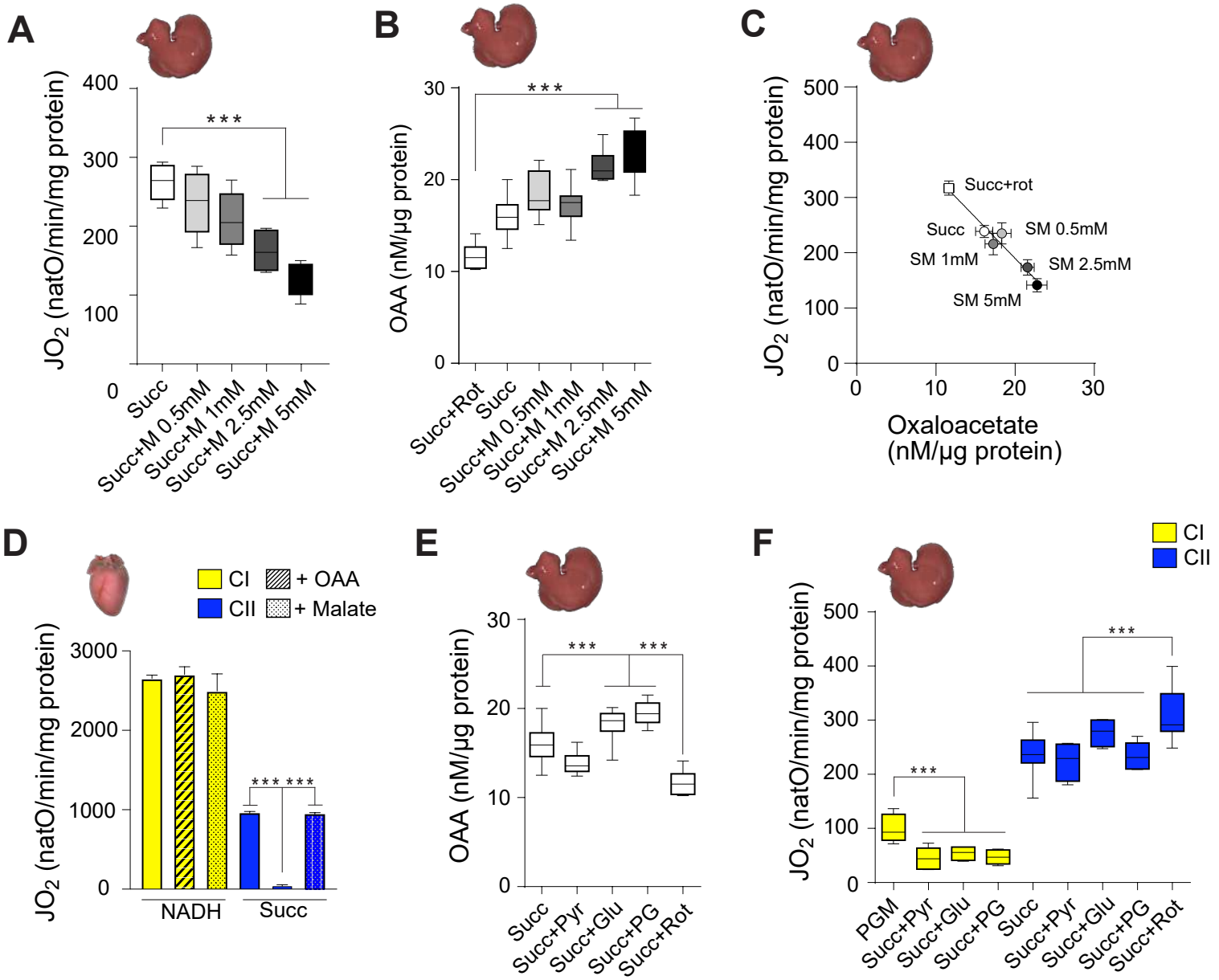

Figure 4S: MDH2 rewires TCA cycle and respiratory chain electrons flow to favour NADH oxidation

(A, B) Oxygen consumption (A) oxaloacetate level (C) assessed with intact liver mitochondria fed with succinate and increased concentration of malate during uncoupled respiration. (n= 3), error bars represent the mean ± SEM. (C) Correlation between mitochondrial oxygen consumption and oxaloacetate levels of intact liver mitochondria isolated fed with succinate and increasing concentration of malate. Error bars represent the mean ± SEM. (D) Oxygen consumption of permeabilised heart mitochondria fed with complex I (NADH, yellow bars) or complex II (Succ, blue bars) substrates ± addition of oxaloacetate (hatched bars) or malate (dotted bars). (n= 4), error bars represent the mean ± SEM. (E) Oxaloacetate levels assessed with intact liver mitochondria in presence of different substrates condition metabolizing endogenously produced OAA (Succ+Glu, Succ+Pyr, Succ+PG). (n= 3), error bars represent the mean ± SEM. (F) Oxygen consumption of intact liver mitochondria fed with indicated substrates conditions (Succ+Pyr, Succ+Glu or Succ+Pyr+Glu). Addition of specific inhibitor of complex I (rotenone) and complex II (AtpeninA5) during uncoupled respiration, determine the complex I driven respiration (yellow bars) or complex II driven respiration (blue bars). (n= 5), error bars represent the mean ± SEM.